Aggregation of Cateslytin β-Sheets on Negatively Charged Lipids Promotes Rigid Membrane Domains. A New Mode of Action for Antimicrobial Peptides?[†]

Frantz Jean-François,[‡] Sabine Castano,[‡] Bernard Desbat,[‡] Benoît Odaert,[‡] Michel Roux,[§] Marie-Hélène Metz-Boutigue,[||] and Erick J. Dufourc*[,‡]

UMR 5248 CBMN, CNRS-Université Bordeaux 1-ENITAB, IECB, Pessac, France, CEA-Saclay, Département de biologie, Gif-sur-Yvette, France, and INSERM Unité 575, Physiopathologie du Système Nerveux, Strasbourg, France

Received March 16, 2008; Revised Manuscript Received April 13, 2008

ABSTRACT: Cateslytin, a positively charged (5+) arginine-rich antimicrobial peptide (bCgA, RSMRLSFRARGYGFR), was chemically synthesized and studied against membranes that mimic bacterial or mammalian systems. Circular dichroism, polarized attenuated total reflection infrared spectroscopy, ^{1}H high-resolution MAS NMR, and ^{2}H and ^{31}P solid state NMR were used to follow the interaction from peptide and membrane points of view. Cateslytin, which is unstructured in solution, is converted into antiparallel β-sheets that aggregate mainly flat at the surface of negatively charged bacterial mimetic membranes. Arginine residues are involved in the binding to negatively charged lipids. Following the interaction of the cateslytin peptide, rigid and thicker membrane domains enriched in negatively charged lipids are found. Much less interaction is detected with neutral mammalian model membranes, as reflected by only minor percentages of β-sheets or helices in the peptide secondary structure. No membrane destruction was detected for both bacterial and mammalian model membranes. A molecular model is proposed in which zones of different rigidity and thickness bring about phase boundary defects that ultimately lead to permeability induction and peptide crossing through bacterial membranes.

The increasing resistance of bacteria to conventional antibiotics makes the development of new modes of treatment essential. Over the past few years, antimicrobial peptides (AP)[1] have been presented as a potential solution to this problem: whereas classical antibiotics act specifically on biosynthetic pathways, antimicrobial peptides may directly destabilize the lipid membrane and constitute a promising alternative strategy for fighting microorganism action. These peptides were first identified in the hemolymph of insects and in the secretion of immune cells (*1*). Insects are indeed the only organisms that produce such peptides as part of a systemic response induced by microorganisms. For mammals, these peptides are part of the innate immune system that constitutes a first host defense line by controlling natural flora (*2*). By 2007, more than 700 different antimicrobial peptides have been identified (see http://aps.unmc.edu/AP/main.php). Most antimicrobial peptides are composed of L-amino acids, with defined α-helix or β-sheet secondary structures. Some are linear, mostly helical, without cysteines, while others contain one or more disulfide bonds, stabilizing β-sheet structure, or both β-sheet and α-helix structures (*3*). In most cases, the peptide mode of action appears to be by direct lysis of the pathogenic cell membrane. The largest and most studied group includes short linear polypeptides (≤40 amino acids) that are devoid of disulfide bridges (*3*). These polypeptides vary considerably in chain length, hydrophobicity, and overall distribution of charges but share a common α-helical structure when associated with phospholipid membranes. Some of these peptides are not cell selective, e.g., the bee venom melittin (*4*), the Moses sole fish lytic peptide pardaxin (*5*), and the human cathelicidin-like LL-37 (*6*), because they are able to lyse both bacterial and mammalian cells. Others are selective either for mammalian cells but not for bacteria (e.g., δ-hemolysin from *Staphylococcus aureus*) (*7*) or vice versa, i.e., cytotoxic to various pathogenic microorganisms but not to normal mammalian cells [e.g., cecropins, isolated from insects (for a review, see ref *8*), and magainins (*9*) and dermaseptins (*10*), both isolated from the skin of frogs]. Despite extensive studies, the mode of action of this group of antibacterial and cytolytic peptides is not fully understood, and the basis for their selectivity toward specific target cells is not known. Nonetheless, two modes of action have been proposed (*3*) for α-helical peptides. The first is (a) the "barrel-stave model" in which bundles of amphipathic helices oligomerize and

[†] This work was supported by the Centre National de la Recherche Scientifique and the Ministère de la Recherche et de l'Enseignement Supérieur. The Aquitaine Region is also thanked for equipment funding.

* To whom correspondence should be addressed: UMR 5248 CBMN, CNRS-Université Bordeaux 1-ENITAB, IECB, 2 rue Robert Escarpit, 33607 Pessac, France. Telephone and fax: +33 (0)5 4000 2218. E-mail: e.dufourc@iecb.u-bordeaux.fr.

[‡] CNRS-Université Bordeaux 1-ENITAB.

[§] CEA-Saclay.

[||] INSERM Unité 575.

[1] Abbreviations: AP, antimicrobial peptides; CgA, chromogranin A; CD, circular dichroism; IR-ATR, infrared attenuated total reflectance; HR-MAS, high-resolution magic angle sample spinning; DMPC, 1,2-dimyristoyl-*sn*-glycero-3-phosphocholine; MLV, large multilamellar vesicles; DMPS, 1,2-dimyristoyl-*sn*-glycero-3-phosphoserine; DMPG, 1,2-dimyristoyl-*sn*-glycero-3-phosphoglycerol; LPC, 1-myristoyl-2-hydroxy-*sn*-glycero-3-phosphocholine; LPG, 1-myristoyl-2-hydroxy-*sn*-glycero-3-phosphoglycerol; TMSP, trimethylsilyl propionate; LUV, large unilamellar vesicles; UHQ, ultrahigh quality; TOCSY, total correlation spectroscopy; NOESY, nuclear Overhauser effect spectroscopy.

10.1021/bi800448h CCC: $40.75
Published on Web 05/24/2008

form transmembrane pores with the hydrophilic residues facing the lumen of the pore. Here, the minimal inhibitory concentration required to dissipate the transmembrane potential should be far below the micromolar concentration, a fact observed for only a few peptides, such as alamethicin, pardaxin, and the α-helix of δ-endotoxin. Alternatively, in the (b) "carpet model", AP act in a detergent-like manner, covering the cell surface until a threshold concentration is reached leading to membrane patch formation with lipids forming toroidal aggregates stabilized by the amphipathic peptides (*11, 12*). Dramatic membrane disruption thus occurs, leading to cell death (*13*).

Antimicrobial peptides resulting from the enzymatic degradation of chromogranin A (CgA) and secreted during stress have been studied recently (*14, 15*). CgA is located in the secretory granules of most endocrine end neuroendocrine cells. As it is cosecreted with several hormones and prohormones, the biological role of this 431-residue (49 kDa) acidic protein is not well-known. The proteolysis of CgA releases several peptides that seem to possess endocrine, paracrine, autocrine, and neuro-immuno-modulatory properties. One of these, named cateslytin ($CgA_{344-358}$) (*16*), was shown to possess new antimicrobial properties (*17*). It was initially characterized for its inhibition of the release of catecholamine from chromaffin cells (*18, 19*). Homology modeling followed by molecular dynamics simulation of bovine catestatin ($bCgA_{342-370}$) performed in a water shell led to a β-strand−loop−β-strand structure (*19*). To the best of our knowledge, its mode of action toward membranes is not known.

To investigate the mode of action of cateslytin, which acts only on bacteria and not on mammals, several physical techniques have been used. Circular dichroism (CD) and polarized ATR (attenuated total reflectance) and ^1H high-resolution magic angle sample spinning (HR-MAS) NMR were used to monitor changes in peptide secondary structure both in solution and in membrane media. ^2H and ^{31}P solid state NMR were used to analyze and quantify membrane structure and dynamics and to further our understanding of the interaction of the peptide with bacterial mimetic membranes, from the membrane viewpoint (*20, 21*). To mimic globally neutral mammalian membranes, 1,2-dimyristoyl-*sn*-glycero-3-phosphocholine (DMPC) water dispersions [large multilamellar vesicles (MLV)] were prepared. To come close to the negative phospholipid charge of *Candida albicans*, a fungus whose growth is perturbed by cateslytin, DMPC/DMPS (1,2-dimyristoyl-*sn*-glycero-3-phosphoserine) (1:1) or DMPC/DMPG (1,2-dimyristoyl-*sn*-glycero-3-phosphoglycerol) (1:1) MLV were made. For HR-MAS NMR, micelles of 1-myristoyl-2-hydroxy-*sn*-glycero-3-phosphocholine (LPC), 1-myristoyl-2-hydroxy-*sn*-glycero-3-phosphoglycerol (LPG), or LPC/LPG (1:1) MLV were used. ^2H NMR experiments were performed with chain-perdeuterated phospholipids. DMPC-$^2H_{54}$/DMPS and DMPC/DMPS-$^2H_{54}$ systems were prepared to follow the respective role of zwitterionic versus charged lipids in a mixed membrane. As some lytic peptides act on membranes depending on their gel or fluid state [e.g., the bee venom toxin melittin (*12, 22*)], NMR and CD have been performed on both sides of their melting temperature (T_m).

MATERIALS AND METHODS

Chemicals. DMPC, DMPS, DMPG, LPC, LPG, chain-perdeuterated DMPC, and DMPS (DMPC-$^2H_{54}$ and DMPS-$^2H_{54}$) were purchased from Avanti Polar Lipids (Alabaster, AL). D_2O-containing trimethylsilyl propionate (TMSP) was purchased from Euriso-Top (Gif-sur-Yvette, France). Bovine cateslytin ($bCgA_{344-358}$, RSMRLSFRARGYGFR) has been synthesized in our laboratory using the Fmoc strategy (*23, 24*) and purified by reverse phase high-performance liquid chromatography (*25*).

Sample Preparation. Mixtures of DMPC and DMPS (1:1 molar ratio) or DMPC and DMPG (1:1) were codissolved in chloroform and methanol (90:10, v/v) and evaporated under vacuum. The residual lipid film was hydrated in distilled water and freeze-dried to remove traces of solvent. This sequence was repeated three times. A final hydration, h [(mass of water)/(mass of lipids and water), in percent], with the buffer was performed to obtain MLV. For NMR and CD samples, h was adjusted to 93 and 98%, respectively, using TKEB buffer [50 mM Tris, 100 mM KCl, and 0.5 mM EDTA (pH 7.4)]. A D_2O buffer [100 mM NaCl and 50 mM Tris (pH 7.5)] was used for ATR with an h of 84%. After being shaken with a "vortex" mixer, the samples were subjected to three freeze−thaw cycles to ensure complete equilibrium. Different lipid:peptide molar ratios (R_i) were used: 15, 50, 100, and 150. Samples for micelle studies were prepared by hydrating the powders in UHQ water at an R_i of 50 (pH 3.4). No peptide degradation was observed at this pH. All peptide concentrations were determined by UV at 280 nm. To reduce light scattering for CD, the MLVs obtained via the protocol described above were submitted to extrusion on a 1.5 mL LIPEX thermobarrel apparatus (Vancouver, BC) at 45 °C in a thermostated bath. Filters of 200 nm were used, and ten passes through the extruder were carried out to produce calibrated LUV.

Circular Dichroism. CD spectra were recorded on a Mark VI Jobin (Longjumeau, France) dichrograph at 0.5 nm intervals over the 180−270 nm wavelength range using a 0.1 mm path length quartz cell. Eight scans were performed. The secondary structure studies were first achieved in water for the following peptide concentrations: 50, 100, 250, 500, and 1000 μM. The second investigation was performed in membranes as a function of temperature. Temperatures were varied from 15 to 45 °C to probe both gel and fluid phases of lipid membranes with a peptide concentration of 1 mM. Experiments were conducted at 15 nm/min, and a stabilization time of 25 min was allowed at each temperature. To estimate the peptide secondary structure content, the relevant CD spectra were converted into mean residue ellipticity, [Θ] (degress square centimeter per decimole), using the relationship $[\Theta] = CD_{meas}/[ClN_R \times 10]$, where C is the concentration in moles per liter, l the cell path length in centimeters, and N_R the number of residues per peptide (*26*). Secondary structure content was estimated from CD spectra using the deconvolution program CDFriend (S. Buchoux, unpublished). This program, developed in the laboratory, uses standard curves obtained for each canonical structure (α-helix, β-sheet, helix II, and random coil) with leucine/lysine (LiKj) peptides with known lengths, secondary structures (*27, 28*), and CD spectra. The program implements a simulated annealing algorithm to obtain the best combination of α-helix, β-sheet,

and random coil that exhibits the lowest normalized root-mean-square deviation (nrmsd) with respect to the experimental spectrum. The experimental error is estimated to be ±5%. Before deconvolution, experimental spectra were smoothed with a 10-point FFT Filter using Origin (Microcal, Northampton, MA). It must be mentioned that we also used available software [CDPro software (http://lamar.colstate.edu/~ssreeram/CDPro)] developed by R. W. Woody and coworkers (*29*) using the basis set containing membrane protein structures and found comparable values. We found our procedure, to be detailed elsewhere, simpler to use (no initial guesses) and well suited for the secondary structure characterization of hydrophobic peptides.

ATR Spectroscopy. Oriented multibilayers were obtained by shearing a pure lipid or mixed cateslytin/lipid water suspension at the diamond ATR crystal surface (golden gate, Eurolabo). ATR spectra were recorded either on a Nicolet (Madison,WI) Magna 550 spectrometer equipped with a MCT detector cooled at 77 K or on a Nicolet Nexus 670 spectrometer equipped with a DTGS detector. The decomposition of the amide I and amide spectral region (1580−1700 cm^{-1}) into individual bands was performed with Peaksolve (GRAMS, version 3.0) and analyzed as a sum of Gaussian/Lorentzian curves, with consecutive optimization of amplitudes, band positions, half-widths, and Gaussian/Lorentzian compositions of the individual bands. Since ATR spectroscopy is sensitive to the orientation of secondary structures (*30*), spectra were recorded with a parallel (p) and perpendicular (s) polarization of the incident light with respect to the ATR plate. Generally, 1000 scans were co-added at a resolution of 8 cm^{-1}, and a two-level zero filling was performed. All the orientation information is then contained in the dichroic ratio R_{ATR} ($=A_p/A_s$, where A_p and A_s represent the band absorbance for the p and s polarization of the incident light, respectively).

Solid State NMR Spectroscopy. NMR experiments were carried out on Bruker (Wissembourg, France) Avance DSX 300 WB and DPX 400 NB spectrometers. ^{31}P NMR spectra were acquired using a phase-cycled Hahn-echo pulse sequence with gated broadband proton decoupling at 162 MHz (*31*). Deuterium NMR experiments on deuterated lipids were performed at 46 MHz by means of a quadrupolar echo pulse sequence (*32*). Typical acquisition parameters were as follows: spectral window of 50 kHz for ^{31}P NMR and 250 kHz for ^{2}H NMR, $\pi/2$ pulse widths ranging from 3 to 5 μs depending on sample, and interpulse delays of 30−40 μs. A recycle delay of 5 s was used for ^{31}P NMR; for ^{2}H NMR experiments, it was set to 2 s. Typically, 2−4K scans were recorded for a deuterium nucleus and 1K transients for a phosphorus nucleus. A line broadening of 50−100 Hz was applied prior to Fourier transformation. Phosphorus chemical shifts were referenced relative to 85% H_3PO_4 (0 ppm). Quadrature detection was used in all cases. Samples were allowed to equilibrate for at least 30 min at a given temperature (ranging from 10 to 50 °C) before the NMR signal was acquired; the temperature was regulated to ±1 °C. All the thermal variations were performed by increasing the temperature. First moments (*20, 33*) were calculated using a C^{2+} homemade routine (S. Buchoux, unpublished) inserted in Microcal Origin to which Bruker NMR data were exported using a proper subroutine.

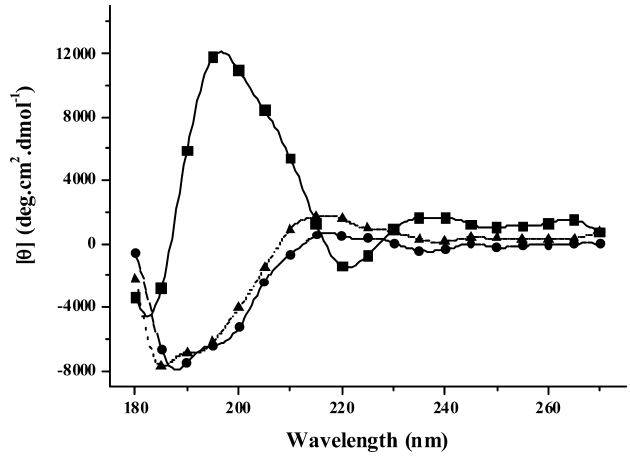

FIGURE 1: Circular dichroism spectra of cateslytin in water at pH 7 (▲), LUV of DMPC for which $R_i = 15$ (●), and 1:1 DMPC/DMPS LUV for which $R_i = 15$ (■). LUVs are in buffer at pH 7.4. Eight scans were accumulated at a scan speed of 15 nm/min at 25 °C.

HR-MAS NMR Spectroscopy. Proton spectra were recorded on a Bruker Avance DSX 500 WB US spectrometer using a 4 mm HR-MAS probe with z-gradient and D_2O lock. The temperature in the rotor was 21 °C after correction for the temperature increase due to magic angle sample spinning at 5 kHz. Chemical shifts were referenced to the singlet (0.00 ppm) of trimethylsilyl propionate (TMSP). Phase-sensitive TOCSY (total correlation spectroscopy) (*35*) and nuclear Overhauser effect spectroscopy (NOESY) (*36*) were conducted using the States−TPPI mode. A 60 ms spin lock time and a 300 ms mixing time were used. Data collection was accomplished on 4096 (t_2) × 512 (t_1) data points with 128 scans per increment. For all experiments, solvent suppression was performed using presaturation (*37*) and Watergate (*38*). Data processing and analysis were accomplished using Topspin.

RESULTS

CD in Solution and in Membranes. Experiments have been performed as a function of temperature in the range of 15−45 °C where no temperature dependence was detected in CD traces, within the experimental error (data not shown). Representative spectra are plotted at 25 °C in Figure 1 and show that the peptide has little structure in a water solution or in DMPC LUV since CD spectra display only a weak minimum at 190 nm. In a water solution, no concentration dependence is noticed in CD measurements, indicated by a lack of significant structural changes between 50 and 1000 μM (data not shown). With the DMPC/DMPS systems, a marked maximum at 196 nm and a minimum at 220 nm suggest the predominance of β-sheet structure. The deconvoluted curves (Table 1) show that peptide secondary structure is made of β-sheet and random coil. In water, the unstructured fraction is 90% and there is only 10% β-sheet. For the DMPC system, the more the lipid proportion is increased (R_i = 15−150), the more the peptide becomes structured (10−30%). On the other hand, for the DMPC/DMPS system, the β-sheet proportion is higher (56%) than in pure DMPC membranes and does not change whatever the lipid:peptide ratio. CD spectra were also acquired for the LPC, LPG, and LPC/LPG (1:1) micellar systems (R_i = 50) (data not shown); cateslytin was found unstructured in micelles.

Polarized ATR in a Powder Solution and in Membranes. ATR experiments were carried out at room temperature in

Table 1: Percentage of Secondary Structure Elements As Determined from CD Measurements on Water and Large Unilamellar Vesicles[a]

	α-helix	β-sheet	random coil
water	0%	11%	89%
DMPC, $R_i = 15$	0%	11%	89%
DMPC, $R_i = 50$	3%	22%	75%
DMPC, $R_i = 100$	0%	31%	69%
DMPC, $R_i = 150$	0%	31%	69%
DMPC/DMPS, $R_i = 15$	0%	56%	44%
DMPC/DMPS, $R_i = 50$	0%	56%	44%
DMPC/DMPS, $R_i = 100$	0%	56%	44%
DMPC/DMPS, $R_i = 150$	0%	56%	44%

[a] Deconvolution of CD spectra was accomplished using the CD Friend deconvolution program (S. Buchoux, unpublished). The accuracy is estimated to within ca. ±5%. $T = 25$ °C.

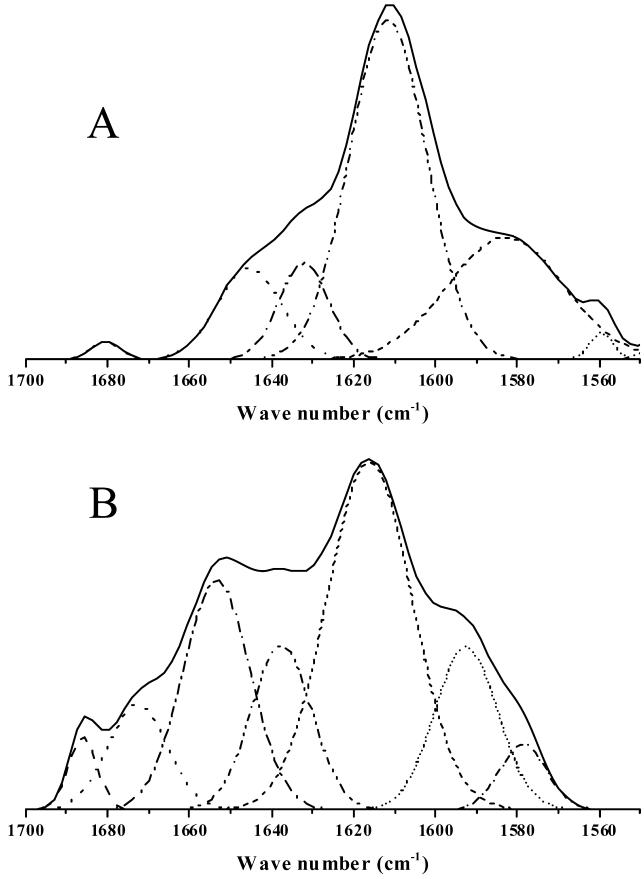

FIGURE 2: P polarization ATR spectra at 25 °C of cateslytin added at an R_i of 15 on multibilayers of DMPC and DMPG (A) and DMPC (B) hydrated by D_2O. Spectral decompositions are shown below experimental spectra (solid lines) with several dashed−dotted lines. Deconvolution was accomplished using Peaksolve (GRAMS, version 3.0).

water and DMPC or DMPC/DMPG (1:1) multibilayer membranes. DMPG was used instead of DMPS to avoid the presence of the carbonyl serine band centered at 1640 cm^{-1} in the amide I region that would prohibit accurate deconvolution. As seen in Figure 2A, the amide I region (1700−1600 cm^{-1}) of cateslytin in membranes displays several bands characteristic of antiparallel β-sheets (1615 and 1685 cm^{-1}), random structures (1635 and 1645 cm^{-1}), α-helices (1654 cm^{-1}), and β-turns (1672 cm^{-1}). The spectrum of the peptide in solution shows a simpler amide I domain. Indeed, two bands are detected in the amide I region (data not shown): a main broad component around 1650 cm^{-1} for the two systems characteristic of unstructured peptide

Table 2: Percentage of Secondary Structure Elements for Cateslytin in Water, DMPC, and DMPC/DMPG (1:1) Membranes, As Obtained from ATR[a]

	α-helix	β-turns	β-sheet	anti-β-sheet	random
water	0%	0%	0%	28%	72%
DMPC, $R_i = 15$	22%	6%	0%	50%	22%
DMPC, $R_i = 150$	31%	7%	0%	37%	25%
DMPC/DMPG, $R_i = 15$	0%	0%	0%	73%	27%
DMPC/DMPG, $R_i = 150$	8%	17%	0%	71%	4%

[a] Deconvolution of ATR spectra was accomplished using Peaksolve (GRAMS, version 3.0). The accuracy is estimated to within ca. ±5%. $T = 25$ °C.

and a band around 1615 cm^{-1} (and 1685 cm^{-1}) characteristic of antiparallel β-sheets. For all these spectra, there is also a component at 1586 cm^{-1} due to the guanidinium antisymmetrical deformation of the arginines in D_2O. Decomposition of the amide I domain after baseline correction and subtraction of residual water (Figure 2B; for DMPC at $R_i = 15$) allows assessment of secondary structure content (Table 2). Decomposition results clearly confirm that cateslytin is mainly unstructured in solution, whereas it folds preferentially into a β-sheet in a lipid environment. The amount of β-structures is ca. 70−90% in DMPC/DMPG membranes and 40−50% in DMPC. A shift of the β-sheet band, indicative of a stronger hydrogen bond as in aggregates, can also be noticed from 1618 to 1613 cm^{-1} when substituting zwitterionic DMPC with anionic DMPC/DMPG membranes. The 20−30% helix character is found only in the presence of the pure DMPC membrane. For all negatively charged systems, a dichroic ratio R_{ATR} of ≈1 has been determined using the amide I′ band at 1685 cm^{-1}. This value is in favor of β-sheets mainly lying flat on the membrane plane (*39*).

^{1}H HR-MAS NMR in LPC, LPG, and LPC/LPG Micelles. The chemical shifts of all protons of cateslytin ($bCgA_{344-358}$) were assigned in LPC, LPG, and LPC/LPG (1:1) micelles using the TOCSY and NOESY sequences (data not shown). Assignments are in general very similar to our previous work in DPC micelles (*25*). Interestingly, the peptide has almost the same signature in chemical shift (Figure 3) in the two negatively charged systems, which differs from that in LPC. This emphasizes that in terms of negative charge titration, saturation is reached. Thus, a half-ratio in negatively charged lipids is sufficient to promote an effect on chemical shifts as important as with a pure negatively charged membrane. A minute analysis of these three systems reveals differences in arginine chemical shifts: the intensity of the H^{ξ} signal is higher in the negatively charged micelles, and the H^{ϵ} signal becomes clearly more unshielded (see the dashed zones in Figure 3). The serine S2 H^N, at 8.7 ppm, which is not seen in neutral micelles due to exchange with water, now appears on LPG and LPC/LPG micelles. NOESY correlations between lipids and the aromatic residues were found on the two-dimensional (2D) maps (data not shown), demonstrating the penetration of tyrosine Y12 and phenylalanine F7 and F14 residues inside the membrane hydrophobic core of LPG and LPG/LPC micelles. Such distance correlations were not detected in LPC.

^{2}H and ^{31}P Solid State NMR of Cateslytin in DMPC and DMPC/DMPS Membranes. Deuterium and phosphorus NMR experiments were performed at several temperatures and lipid-to-peptide ratios using multilamellar vesicles of DMPC-$^2H_{54}$, DMPC-$^2H_{54}$ and DMPS (1:1), and DMPS-$^2H_{54}$ and

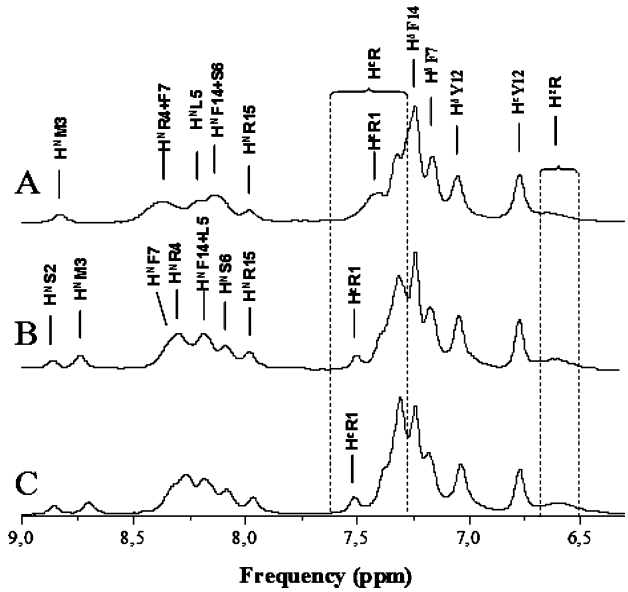

FIGURE 3: ^{1}H HR-MAS NMR chemical shifts (parts per million) of cateslytin ($bCgA_{344-358}$) externally added at an R_i of 50, at 294 K, in LPC (A), LPC/LPG (1:1) (B), and LPG (C) micelles, relative to TMSP (0 ppm). The spin rate was 5 kHz for all experiments. Assignment of resonances was accomplished using TOCSY and ROESY sequences (see the text). Dotted regions highlight chemical shifts variations for cationic residues, upon addition of cateslytin.

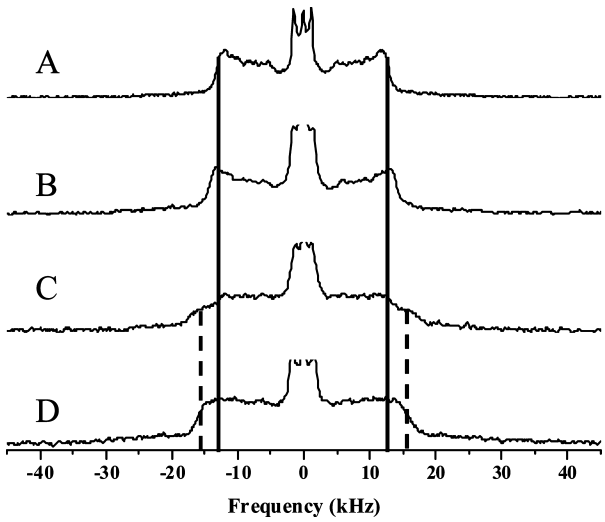

FIGURE 4: Comparison of ^{2}H NMR powder spectra of DMPC mixed with DMPS (1:1 molar ratio) without (A and B) or with (C and D) cateslytin at an R_i of 15 and 37 °C. (A and C) DMPC is deuterated. (B and D) DMPS is deuterated. The small isotropic line (less than 5%) has been chopped off to highlight powder pattern changes. Vertical lines are eye guides for lipid ordering at plateau positions for pure systems (dashed) and domainlike systems in the presence of peptide.

DMPC (1:1). Representative spectra recorded in the absence of cateslytin, at 37 °C (above the T_m), are shown in Figure 4 for the DMPC/DMPS membrane, either with labeled DMPC (Figure 4A) or with labeled DMPS (Figure 4B). All spectra exhibit an axially symmetric line shape indicating that the membrane is in the fluid state (fast intra- and intermolecular axially symmetric motions) (*20, 21*). An isotropic line representing less than 5% of the total spectral area is observed on almost all spectra; it is assigned to a small quantity of rapidly tumbling small vesicles occurring during the sample preparation. It is chopped off to show

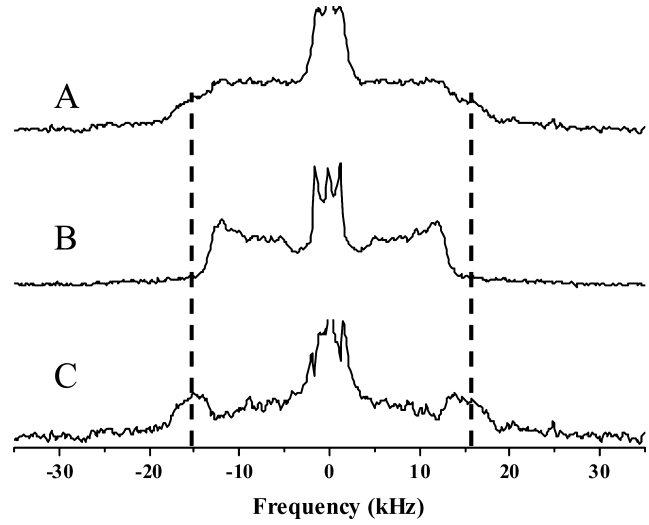

FIGURE 5: Comparison of the effect of cateslytin ($R_i = 15$) on fluid phase DMPC-$^2H_{54}$/DMPS micelles (37 °C): (A) with cateslytin and (B) without cateslytin. In panel C is shown the subtraction of 50% B from A. The vertical dashed line is an eye guide highlighting the same plateau quadrupolar splittings for panels A and C.

details on powder patterns on which one can measure splittings for the outermost doublet (26−27 kHz), representing the "plateau" positions (labeled carbons C_3−C_8) and reporting for lipid dynamics near the interface, and for the inner doublet (3 kHz), giving information about the membrane center (methyl terminal, C_{14}). Intermediate labeled positions show splittings between 3 and 26 kHz. The variation of quadrupolar splitting with labeled carbon positions depicts the well-known gradient of internal membrane ordering (microfluidity) (*40*). Addition of cateslytin at an R_i of 50 (not shown) leads to hardly measurable changes. Further addition of cateslytin [$R_i = 15$ (Figure 4C,D)] leads to spectra wider than those recorded in the absence of peptide. A small isotropic line is also detected, as in control spectra. The spectrum obtained with labeled DMPC (Figure 4C) clearly shows two spectral components in slow exchange on the NMR time scale (tens of microseconds), one resembling that of the cateslytin-free system (Figure 4A) and a wider one, which can be better seen by using a subtraction procedure (*41*). For clarity, the system with labeled DMPC in the presence and absence of cateslytin is plotted again in panels A and B of Figure 5, and Figure 5C shows the result of the operation (Figure 5A − 0.5 × Figure 5B); a quadrupolar splitting of 31 ± 1 kHz can thus be measured for the plateau positions. The spectrum obtained with labeled DMPS (Figure 4D) shows only one powder pattern, much wider than without peptide. Plateau and methyl quadrupolar splittings of 31 ± 1 and 3.7 ± 0.5 kHz are detected, respectively. It is clearly seen that either DMPC or DMPS reports the same quadrupolar splitting increase, within the experimental error, upon the action of cateslytin. The only variance is that all DMPS is affected whereas only half of DMPC undergoes an increase in ordering. The phenomenon appears to be stable enough because a temperature increase to 50 °C does not change spectral shapes (data not shown). At low temperatures, the gel phase spectra obtained in the absence of peptide become also wider upon addition of cateslytin (not shown). Because of the shape and broadness of spectra at such temperatures, measurement and spectral subtraction are not accurately feasible. Addition of cateslytin to pure DMPC

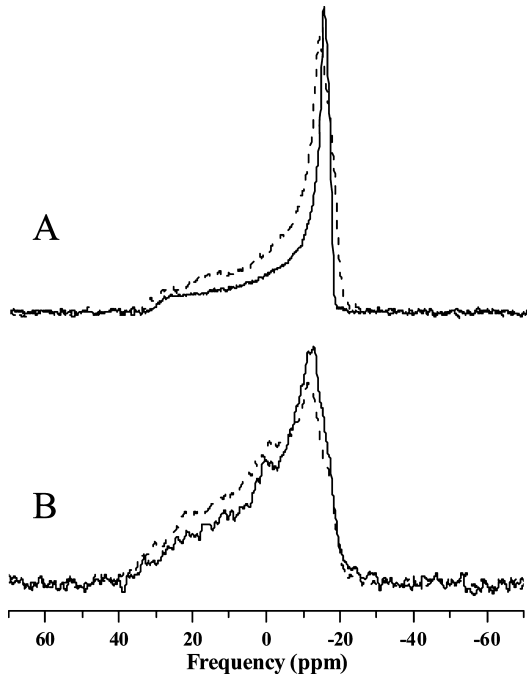

FIGURE 6: Wideline proton-decoupled ^{31}P NMR spectra of (A) DMPC and (B) DMPC/DMPS (1:1) multilamellar vesicles containing pure lipids (solid lines) or lipids with cateslytin peptide added at an R_i of 15 (dashed lines) and 37 °C. Spectra are in the absolute intensity mode, within panel A and within panel B.

membranes [R_i = 15 (data not shown)] did not markedly modify spectra at high and low temperatures. However, changes appeared near the phase transition temperature (T_m = 23 °C). From the full thermal variation of the first spectral moment (not shown), a decrease in T_m of ca. 5 °C is estimated.

^{31}P NMR was also used to report on cateslytin−membrane interactions from the point of view of membrane surface. Figure 6 shows axially symmetric spectra at 37 °C for DMPC and DMPC/DMPS systems, in the absence and presence of peptide (R_i = 15). All experimental conditions were kept the same, especially the same amount of lipids in the sample and the same number of scans. Spectra are plotted in the absolute intensity mode, so a quantitative comparison can be made. A small isotropic line is detected in some spectra. Because its intensity is very weak, it indicates that no major macroscopic changes occur (no formation isotropic phases); it can therefore be neglected. Powder spectra in the presence of cateslytin (dashed lines) are less intense but clearly broader, the area staying the same, within experimental error. This is reflected using the second-moment calculation, M_2. For the DMPC system, M_2 is (200 ± 20) × 10^6 Hz^2 (7620 ± 76 ppm^2) without peptide and increases to (240 ± 20) × 10^6 Hz^2 (9150 ± 76 ppm^2) with peptide. For the DMPC/DMPS system, M_2 varies from (130 ± 20) × 10^6 Hz^2 (4960 ± 76 ppm^2) to (180 ± 20) × 10^6 Hz^2 (6860 ± 76 ppm^2) in the presence of cateslytin. This suggests either an intermediate rate of exchange between spectra of different orientational ordering or the incoming of slow motions such as bilayer collective modes (*20, 21*).

DISCUSSION

There are three major outcomes of our study. (i) Cateslytin adopts a dominant β-sheet character upon interaction with negatively charged membranes. (ii) Arginine residues are involved in the interaction with negatively charged membranes. (iii) Membrane regions of increased rigidity are observed only with negatively charged systems. These findings will be discussed below, and a scheme will be proposed to account for antimicrobial peptide action, at the molecular level.

Cateslytin Switches to Antiparallel β-Sheet Aggregates on Negatively Charged Membranes. Both CD and ATR experiments clearly show that cateslytin adopts a major β-sheet character only on negatively charged membranes, whereas it is essentially unstructured in water as most short linear antimicrobial peptides. As one can see in Figure 7, the β-sheet structure gives to this peptide a high amphipathic character in accordance with an interfacial interaction on a membrane. On zwitterionic membranes, the β-character is detected to a lesser extent with additional random and helix secondary structures depending upon the technique used. Moreover, polarized ATR indicates that antiparallel β-sheet aggregates, when detected, are mostly lying flat at the membrane interface. However, as shown in previous studies, this average orientation found by ATR-FTIR does not banish the presence of some peptides at other orientations with respect to the membrane plane (*42*). Although the same main trend is reported by both techniques, CD and ATR, there are some small discrepancies in the amounts of secondary structures calculated. They may be attributed to intrinsic errors in deconvolution techniques (ca. ±5%) and may also be associated with the much higher concentration of the ATR sample, which results in a lower hydration level, i.e., 84% hydration (260 mM) compared to 98% hydration (35 mM) for the CD samples. Because peptide/membrane systems are sheared on the ATR crystal surface, to obtain oriented membranes, this induces an additional small mechanical force of interaction that is not present when CD samples are prepared. One may then expect amplification of the tendency of the peptide to penetrate into the membrane core and hence greater secondary structure character. Helix is not found, within experimental error, with negatively charged membranes, where the strong electrostatic interaction with the positively charged peptide clearly stabilizes β-sheets lying flat at the interface. Such a phenomenon has already been reported with the highly cationic polylysin undergoing a random-to-β-sheet transition upon contact with negatively charged dimyristoylphosphatidic acid membranes (*43*). Zwitterionic membranes do not attract cateslytin as efficiently, as seen by the higher percentage of random structures detected. This is particularly clear in CD experiments where elevated amounts of peptide lead to high percentages of disordered structures (Table 1; R_i = 15) in a way very similar to that found in water. It is also worth noting the absence of folding in LPG or LPC/LPG micelles: this reveals that the peptide cannot form structure by itself on highly curved lipid surfaces. The positions of the antiparallel β-sheet amide I band at 1613 and 1618 cm^{-1} for DMPC/DMPG and DMPC multibilayers, respectively, are characteristic of a very strong hydrogen bond in β-sheet aggregates (*44*). The observation of a very low value for the amide I vibration may be linked to a stronger β-sheet aggregation in the presence of a negatively charged interface. The absence of peptide β-turns in the DMPC system and at high DMPC/DMPG:cateslytin ratios (R_i = 15; large quantity of peptide) suggests that antiparallel β-sheets are formed through inter- rather than

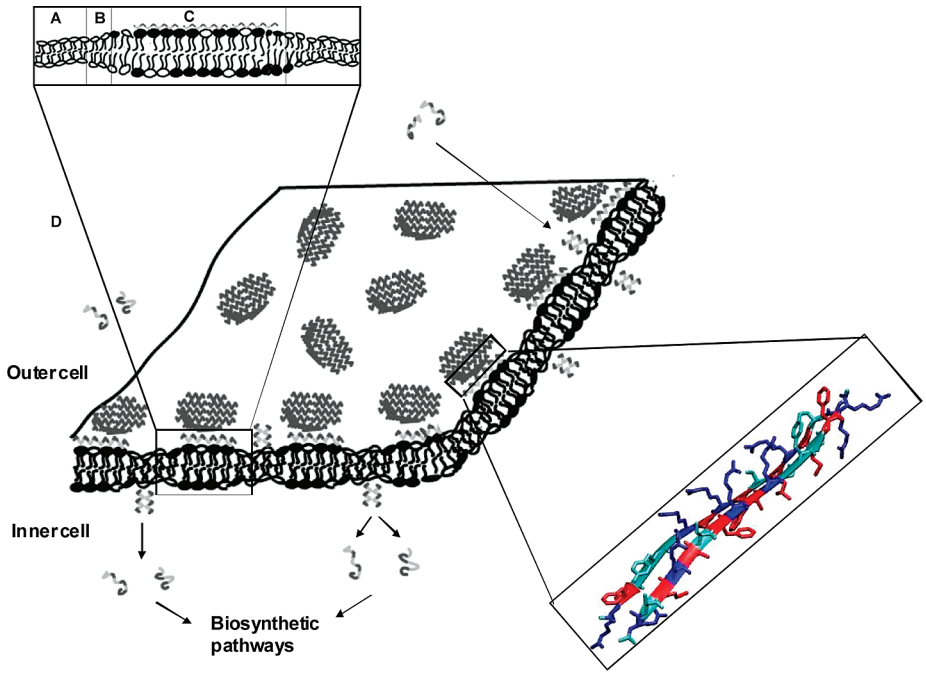

FIGURE 7: Model for interaction of cateslytin with bacterial-like membrane domains. Peptides are unstructured in solution (D) and adopt a β-sheet conformation upon interaction with negatively charged membranes (C). At the membrane, the peptides aggregate to form β-sheet plates leading to formation of rigid (thicker) domains (C) enriched with negatively charged lipids (see the top inset). Passage across the membrane could occur through phase boundary defects (B) between thin (DMPC, A) and thick (DMPS, DMPC, C) membrane domains. The bottom inset shows VMD software representation of two antiparallel β-sheet cateslytin peptides built and minimized using Macromodel. The minimization was performed in water using the Amber force field and TNCG method. Amino acids are colored as a function of their hydrophobicity: basic residues (arginines) in blue, polar residues in cyan, and hydrophobic residues in red.

intrapeptide interactions. At a low ratio (R_i = 150), where there are not enough neighbors, intrapeptide interactions through β-turns would be necessary for antiparallel β-sheet formation, as experimentally observed.

Arginine Residues Play a Determinant Role upon Interaction with Negatively Charged Membranes. The HR-MAS ^{1}H NMR results clearly indicate that arginines and aromatic residues are in close contact with lipid resonances, but only on negatively charged systems. As one can see in Figure 3, there is less exchange between arginine H^{ξ} and water in LPG or LPC/LPG systems (narrower resonances). Deeper penetration of charged residues into the membrane can account for the fact that the H^{ξ} protons are less available for exchange with water. With regard to arginine H^{ϵ} and particularly that belonging to arginine 1, the observed unshielding can be explained by a lesser contact with water. On the other hand, the serine 2 H^N resonance is not detected in the zwitterionic system because of exchange with water: the peptide is no longer attracted by the membrane through the favorable electrostatic interaction. Though the electrostatic interaction between positively charged residues and negatively charged lipid head groups appears to be responsible for binding, the aromatic residues are also involved in the stabilization of the lipid−peptide complex. The effect is less important on chemical shielding of phenylalanine or tyrosine resonances, but through-space interaction is assessed with lipid resonances of the interfacial region and even down in the bilayer core. A two-step mechanism could be proposed: (i) strong electrostatic interaction and (ii) a further stabilization through van der Waals forces between aromatic residues and hydrophobic lipid chains. On zwitterionic systems, the electrostatic interaction is absent; the van der Waals forces remain but are less effective for peptide stabilization at the membrane.

Ordered Lipid Domains Are Induced by Cateslytin on "Bacterial-like" Membranes. A clear spectral width and quadrupolar splitting increase are observed with deuterium NMR when cateslytin is added to negatively charged (DMPS/DMPC) membranes. This is observed at both low and high temperatures, but high-temperature spectra are better resolved and bring more details. Of interest is the fact that in a manner independent of the lipid reporter used (DMPS-$^2H_{54}$ or DMPC-$^2H_{54}$), the same ca. 20% increase in quadrupolar splitting is observed at 37 °C. It is remarkable that all DMPS undergo the increase in splitting whereas a composite spectrum is observed with DMPC. Decomposition shows that there are in fact two DMPC spectra in slow exchange, one representative of a peptide-free membrane and the other with the 20% increase in splitting. Because acyl chains are perdeuterated, and because the observed quadrupolar splittings are proportional to carbon−deuterium bond ordering, a global increase in quadrupolar splitting can be associated with an increase in hydrophobic core membrane ordering. This in turn has been shown to correspond to a thickening by a few angstroms of the bilayer (*45–47*). This effect is tentatively sketched in Figure 7 where the membrane thickening due to cateslytin is depicted. Because all DMPS and half of DMPC show the same increase in ordering (Figures 4D and 5B), they may be placed in the same thick membrane domain (Figure 7C). The other half of DMPC, free from the interaction (Figure 4A), may be placed outside the rigid domain (Figure 7A). There may be a junction region (Figure 7 B), mainly composed of rigid DMPC, slowly exchanging between the free pool and the thick domain. Although the thickening effect may appear subtle, we must remember that the elastic properties of lipid bilayers depend on the square of their thickness (*48*), meaning that an increase

of a few angstroms will change substantially the membrane mechanical properties (deformation, permeability, etc.). The increase in membrane thickness can be linked to the neutralization of the lipid headgroup as reported for other basic peptides (*43*) and is at variance with what has been reported for melittin, δ-hemolysin, and magainin, which have a tendency to fluidize membranes at high temperatures (*11, 13, 49*). In our case, it clearly appears that DMPS-enriched membrane domains coexist with DMPC regions that are depleted in negatively charged lipids and do not perceive the cateslytin ordering action. There is no such effect with pure zwitterionic lipid DMPC: almost no ordering is detected. The only observation is a ca. 5 °C lowering in the lipid phase transition upon addition of peptide, evidencing a definite interaction with mammalian-like membranes but with a much smaller membrane perturbation. The differential ordering effect between neutral and acidic membrane interfaces may be attributed to the penetration of aromatic residues into the bilayer core; the deeper the insertion (especially with negatively charged lipids), the greater the ordering. The results obtained with phosphorus NMR report only a spectral broadening, suggesting either a fast-to-intermediate exchange regime between domains or the income of low-frequency modes of motion (*21, 50*). There is no dominant isotropic line in phosphorus or deuterium spectra, clearly indicating that membrane integrity is maintained upon interaction with cateslytin. This is at variance with what has been reported, for instance, for melittin, the bee venom amphipathic helical peptide known to induce the direct lysis of cell membranes (*11, 13, 51*), where formation of small bilayered discoidal particles of a few hundred angstroms promoted conversion of solid state NMR spectra into isotropic lines.

Biological Implications: Hypothetical Mode of Action. Assembling the findings discussed above into a molecular model leads to the schematics of Figure 7. With strong and leading electrostatic interaction between basic residues and acidic lipid headgroups at membrane surfaces, as found in bacterial systems, cateslytin, which is unstructured in solution, aggregates as patches of antiparallel amphipathic β-sheets. These domains enriched in negatively charged lipids become ordered; i.e., the level of lipid anisotropic diffusion is greatly lowered, mainly due to the insertion of aromatic residues into the hydrophobic bilayer core. The presence of these domains generates zones that are thicker in the membrane. These zones of different rigidity and thickness bring about phase boundary defects that could promote leakage as already proposed by several authors in the case of lipid segregation by a peptide (*52*), temperature-induced gel−fluid phase boundary defects (*53*), and ethanol action (*54*). Thus, as reported in the case of biological systems (*17*), cateslytin could pass through the membrane and interact with crucial biological pathways, as do other arginine-rich peptides (*55*). This could be accomplished by β-barrel oligomerization favored by phase boundary defect zones so that the positive charges are not in contact with the hydrophobic core of the membrane. However, this latter hypothesis is at present out of reach and requires more experimental evidence from studies in progress in our laboratory. It is noteworthy that the mechanism sketched in Figure 7 is at variance with the two mechanisms of antimicrobial peptide action proposed by Y. Shai (*3*). In the carpet model, the membrane would have formed small membranous particles that would have given rise to a dominant isotropic line in solid state NMR, which is not observed. The barrel-stave model is specific for helices but could be adapted to β-barrel pores as in the case of antiparallel β-sheet peptides as found here (*56*).

The combined results of CD, ATR, and solid state NMR allowed us to decipher the mode of action of cateslytin on systems modeling mammalian and bacterial membranes. Both the peptide and lipid points of view can be followed, providing molecular details about the interaction. Changes in secondary structure and membrane physical and dynamical properties are easily followed in a nonperturbing manner.

ACKNOWLEDGMENT

We gratefully thank Axelle Grelard and Benoît Odaert (UMR 5248 CBMN, Pessac, France) for their help in setting up the NMR platform and Kathel Bathany (UMR 5248 CBMN) for the mass spectrometry analyses.

REFERENCES

1. Hoffmann, J. A., Reichhart, J. M., and Hetru, C. (1996) Innate immunity in higher insects. *Curr. Opin. Immunol. 8*, 8–13.
2. Zasloff, M. (2002) Antimicrobial peptides of multicellular organisms. *Nature 415*, 389–395.
3. Shai, Y. (1999) Mechanism of the binding, insertion and destabilization of phospholipid bilayer membranes by α-helical antimicrobial and cell non-selective membrane-lytic peptides. *Biochim. Biophys. Acta 1462*, 55–70.
4. Blondelle, S. E., and Houghten, R. A. (1991) Hemolytic and Antimicrobial Activities of the Twenty-Four Individual Omission Analogues of Melittin. *Biochemistry 30*, 4671–4678.
5. Shai, Y., Bach, D., and Yanovsky, A. (1990) Channel Formation Properties of Synthetic Pardaxin and Analogues. *J. Biol. Chem. 265*, 20202–20209.
6. Oren, Z., Lerman, J. C., Gudmundsson, G. H., Agerberth, B., and Shai, Y. (1999) Structure and organization of the human antimicrobial peptide LL-37 in phospholipid membranes: Relevance to the molecular basis for its non-cell-selective activity. *Biochem. J. 341*, 501–513.
7. Birkbeck, T. H., and Whitelaw, D. D. (1980) Immunogenicity and molecular characterization of Staphylococcal δ Haemolysin. *J. Med. Microbiol. 13*, 213–221.
8. Hultmark, D. (1993) Immune reactions in *Drosophila* and other insects: A model for innate immunity. *Trends Genet. 9*, 151–186.
9. Zasloff, M. (1987) Magainins, a class of antimicrobial peptides from *Xenopus* skin: Isolation, characterization of two active forms, and partial cDNA sequence of a precursor. *Proc. Natl. Acad. Sci. U.S.A. 84*, 5449–5453.
10. Pouny, Y., Rapaport, D., Mor, A., Nicolas, P., and Shai, Y. (1992) Interaction of antimicrobial dermaseptin and its fluorescently labeled analogues with phospholipid membranes. *Biochemistry 31*, 12416–12423.
11. Dufourc, E. J., Smith, I. C. P., and Dufourcq, J. (1986) Molecular details of melittin-induced lysis of phospholipid membranes as revealed by deuterium and phosphorus NMR. *Biochemistry 25*, 6448–6455.
12. Pott, T., and Dufourc, E. J. (1995) Action of melittin on the DPPC-cholesterol liquid-ordered phase: A solid state ^{2}H and ^{31}P-NMR study. *Biophys. J. 68*, 965–977.
13. Dufourc, E. J., Bonmatin, J. M., and Dufourcq, J. (1989) Membrane structure and dynamics by ^{2}H- and ^{31}P-NMR. Effects of amphipatic toxins on phospholipid and biological membranes. *Biochimie 71*, 117–123.
14. Metz-Boutigue, M. H., Goumon, Y., Lugardon, K., Strub, J. M., and Aunis, D. (1998) Antibacterial peptides are present in chromaffin cell secretory granules. *Cell. Mol. Neurobiol. 18*, 249–266.
15. Metz-Boutigue, M. H., Kieffer, A. E., Goumon, Y., and Aunis, D. (2003) Innate immunity: Involvement of new neuropeptides. *Trends Microbiol. 11*, 585–592.
16. Taylor, C. V., Taupenot, L., Mahata, S. K., Mahata, M., Wu, H., Yasothornsrikul, S., Toneff, T., Caporale, C., Jiang, Q., Parmer, R. J., Hook, V. Y., and O'Connor, D. T. (2000) Formation of the catecholamine release-inhibitory peptide catestatin from chromog-

ranin A. Determination of proteolytic cleavage sites in hormone storage granules. *J. Biol. Chem. 275*, 22905–22915.
17. Briolat, J., Wu, S. D., Mahata, S. K., Gonthier, B., Bagnard, D., Chasserot-Golaz, S., Helle, K. B., Aunis, D., and Metz-Boutigue, M. H. (2005) New antimicrobial activity for the catecholamine release-inhibitory peptide from chromogranin A. *Cell. Mol. Life Sci. 62*, 377–385.
18. Mahata, S. K., O'Connor, D. T., Mahata, M., Yoo, S. H., Taupenot, L., Wu, H., Gill, B. M., and Parmer, R. J. (1997) Novel autocrine feedback control of catecholamine release. A discrete chromogranin a fragment is a noncompetitive nicotinic cholinergic antagonist. *J. Clin. Invest. 100*, 1623–1633.
19. Tsigelny, I., Mahata, S. K., Taupenot, L., Preece, N. E., Mahata, M., Khan, I., Parmer, R. J., and O'Connor, D. T. (1998) Mechanism of action of chromogranin A on catecholamine release: Molecular modeling of the catestatin region reveals a β-strand/loop/β-strand structure secured by hydrophobic interactions and predictive of activity. *Regul. Pept. 77*, 43–53.
20. Dufourc, E. J. (2006) Solid state NMR in biomembranes, in *Chemical Biology*, (B., L., Woscholski, R., and Rosser, C. A., Eds.) pp 113−131, John Wiley & Sons, Ltd., London.
21. Dufourc, E. J., Mayer, C., Stohrer, J., Althoff, G., and Koth, G. (1992) Dynamics of phosphate head groups in biomembranes. Comprehensive analysis using phosphorus-31 nuclear magnetic resonance lineshape and relaxation time measurements. *Biophys. J. 61*, 42–47.
22. Faucon, J. F., Bonmatin, J. M., Dufourcq, J., and Dufourc, E. J. (1995) Acyl chain length dependence in the stability of melittin-phosphatidylcholine complexes. A ligth scattering and ^{31}P-NMR study. *Biochim. Biophys. Acta 1234*, 235–243.
23. Khemtémourian, L., Bathany, K., Schmitter, J. M., and Dufourc, E. J. (2006) Fast and quantitative recovery of hydrophobic and amphipathic peptides after incorporation into phospholipid membranes. *Anal. Chem. 78*, 5348–5353.
24. Khemtémourian, L., Sani, M. A., Bathany, K., Gröbner, G., and Dufourc, E. J. (2005) Synthesis and secondary structure in membranes of the Bcl-2 anti-apoptotic domain BH4. *J. Pept. Sci. 12*, 58–64.
25. Jean-Francois, F., Khemtemourian, L., Odaert, B., Castano, S., Grelard, A., Manigand, C., Bathany, K., Metz-Boutigue, M. H., and Dufourc, E. J. (2007) Variability in secondary structure of the antimicrobial peptide cateslytin in powder, solution, DPC micelles and at the air-water interface. *Eur. Biophys. J. Biophys. Lett. 36*, 1019–1027.
26. Berova, N., Nakanishi, K., and Woody, R. W. (2000) *Circular dichroism principles and applications*, Wiley-VCHNew York.
27. Castano, S., Desbat, B., and Dufourcq, J. (2000) Ideally amphipathic β-sheeted peptides at interfaces: Structure, orientation, affinities for lipids and hemolytics activities. *Biochim. Biophys. Acta 1463*, 65–80.
28. Castano, S., Desbat, B., Laguerre, M., and Dufourcq, J. (1999) Structure orientation and affinity for interface and lipids of ideally amphipathics lytics LiKi(i = 2j) peptides. *Biochim. Biophys. Acta 1416*, 176–194.
29. Sreerama, N., and Woody, R. W. (2000) Estimation of protein secondary structure from circular dichroism spectra: Comparison of CONTIN, SELCON, and CDSSTR methods with an expanded reference set. *Anal. Biochem. 287*, 252–260.
30. Goormaghtigh, E., Raussens, V., and Ruysschaert, J. M. (1999) Attenuated total reflection infrared spectroscopy of proteins and lipids in biological membranes. *Biochim. Biophys. Acta 1422*, 105–185.
31. Rance, M., and Byrd, R. A. (1983) Obtaining high-fidelity spin-1/2 powder spectra in anisotropic media: Phase-Cycled Hahn echo spectroscopy. *J. Magn. Reson. 52*, 221–240.
32. Davis, J. H., Jeffrey, K. R., Bloom, M., Valic, M. I., and Higgs, T. P. (1976) Quadrupolar echo deuteron magnetic resonance spectroscopy in ordered hydrocarbon chains. *Chem. Phys. Lett. 42*, 390–394.
33. Bloom, M., Davis, J. H., and Mackay, A. L. (1981) Direct determination of the oriented sample NMR spectrum from the powder spectrum for systems with a local axial symmetry. *Chem. Phys. Lett. 80*, 198–202.
34. Deleted in proof.
35. Bax, A., and Davis, D. G. (1985) MLEV-17-based two-dimensional homonuclear magnetization transfer spectroscopy. *J. Magn. Reson. 65*, 355–360.
36. Bax, A., and Davis, D. G. (1985) Practical aspects of two-dimensional transverse NOE spectroscopy. *J. Magn. Reson. 63*, 207–213.
37. Hore, P. J. (1983) Solvent suppresion in fourier transform nuclear magnetic resonance. *J. Magn. Reson. 55*, 283–300.
38. Piotto, M., Saudek, V., and Sklenar, V. (1992) Gradient tailored excitation for single-quantum NMR-spectroscopy of aquous-solutions. *J. Biomol. NMR 2*, 661–665.
39. Castano, S., and Desbat, B. (2005) Structure and orientation study of fusion peptide FP23 of gp41 from HIV-1 alone or inserted into various lipid membrane models (mono-, bi- and multibi-layers) by FT-IR spectroscopies and Brewster angle microscopy. *Biochim. Biophys. Acta 1715*, 81–95.
40. Seelig, J. (1977) Deuterium magnetic resonance: Theory and application to lipid membranes. *Q. Rev. Biophys. 10*, 353–418.
41. Vist, M. R., and Davis, J. H. (1990) Phase equilibria of cholesterol dipalmitoylphosphatidylcholine mixtures: ^{2}H-nuclear magnetic resonance and differential scanning calorimetry. *Biochemistry 29*, 451–464.
42. Matsuzaki, K., Murase, O., Fujii, N., and Miyajima, K. (1995) Translocation of a Channel-Forming Antimicrobial Peptide, Magainin-2, across Lipid Bilayers by Forming a Pore. *Biochemistry 34*, 6521–6526.
43. Laroche, G., Dufourc, E. J., Pézolet, M., and Dufourcq, J. (1990) Coupled changes between lipid order and polypeptide conformation at the membrane surface. A ^{2}H NMR and Raman study of polylysine-phosphatidic acid systems. *Biochemistry 29*, 6460–6465.
44. Zandomeneghi, G., Krebs, M. R. H., Mccamon, M. G., and Fändrich, M. (2004) FTIR reveals structural differences between native β-sheet proteins and amyloid fibrils. *Protein Sci. 13*, 3314–3321.
45. Douliez, J. P., and Dufourc, E. J. (1995) Comparison of methods to determine aliphatic chain length in biomembranes from selectively or perdeurated systems. A ^{2}H-NMR study. *J. Chim. Phys. 92*, 1721–1726.
46. Douliez, J. P., Leonard, A., and Dufourc, E. J. (1995) Restatement of order parameters in biomembranes: Calculation of C-C bond order parameters from C-D quadrupolar splittings. *Biophys. J. 68*, 1727–1739.
47. Douliez, J. P., Leonard, A., and Dufourc, E. J. (1996) Conformational order of DMPC sn-1 versus sn-2 chains and membrane thickness: An approach to molecular protrusion by solid-state ^{2}H-NMR and neutron diffraction. *J. Phys. Chem. 100*, 18450–18457.
48. Fernandez-Puente, L., Bivas, I., Mitov, M. D., and Méléard, P. (1994) Temperature and chain length effects on bending elasticity of phosphatidylcholine bilayers. *Europhys. Lett. 28*, 181–186.
49. Bechinger, B. (1999) The structure, dynamics and orientation of antimicrobial peptides in membranes by multidimensional solid-state NMR spectroscopy. *Biochim. Biophys. Acta 1462*, 157–183.
50. Meier, P., Sachse, J. H., Brophy, P. J., Marsh, D., and Kothe, G. (1987) Integral membrane proteins significantly decrease the molecular motion in lipid bilayers: A deuteron NMR relaxation study of membranes containing myelin proteolipid apoprotein. *Proc. Natl. Acad. Sci. U.S.A. 84*, 3704–3708.
51. Dufourc, E. J., Faucon, J. F., Fourche, G., Dufourcq, J., Gulik-Krywicki, T., and Le Maire, M. (1986) Reversible disc-to-vesicle transition of melittin-DPPC complexes triggered by the phospholipid acyl chain melting. *FEBS Lett. 201*, 205–209.
52. Epand, R. F., Schmitt, M. A., Gellman, S. H., and Epand, R. M. (2006) Role of membrane lipids in the mechanism of bacterial species selective toxicity by two α/β-antimicrobial peptides. *Biochim. Biophys. Acta 1758*, 1343–1350.
53. Hays, L. M., Crowe, J. H., Wolkers, W., and Rudenko, S. (2001) Factors affecting leakage of trapped solutes from phospholipid vesicles during thermotropic phase transitions. *Cryobiology 42*, 88–102.
54. Komatsu, H., and Okada, S. (1995) Increased permeability of phase-separated liposomal membranes with mixtures of ethanol-induced interdigitated and non-interdigitated structures. *Biochim. Biophys. Acta 1237*, 169–175.
55. Futaki, S. (2005) Membrane-permeable arginine-rich peptides and the translocation mechanisms. *Adv. Drug Delivery Rev. 57*, 547–558.
56. Mani, R., Cady, S. D., Tang, M., Waring, A. J., Lehrer, R. I., and Hong, M. (2006) Membrane-dependent oligomeric structure and pore formation of a β-hairpin antimicrobial peptide in lipid bilayers from solid-state NMR. *Proc. Natl. Acad. Sci. U.S.A. 103*, 16242–16247.

BI800448H